J Electroceram (2008) 20:95–105
DOI 10.1007/s10832-007-9364-3

Electrical properties of PZT piezoelectric ceramic at high temperatures

Z. Gubinyi · C. Batur · A. Sayir · F. Dynys

Received: 18 June 2007 / Accepted: 9 November 2007 / Published online: 4 December 2007

Abstract Advanced aeronautic and space structures need active components that can function at high frequencies and temperatures. Piezoelectric materials can provide frequency response but their use at elevated temperatures is limited. The reason for the lack of insertion of piezoelectric for high temperature active component and sensors are two fold. First, the database of piezoelectric properties that describe the piezoelectric constants is lacking for high temperatures engineering applications. Most studies measure the dielectric constants to determine the Curie temperature but do not provide piezoelectric coefficients as a function of temperature. Second, piezoelectric materials with Curie temperature (T_C) exceeding 500 °C are sought for aeronautics and aerospace applications. This investigation describes a measurement system that captures the impedance dependence upon temperature for piezoelectric materials. Commercially available lead zirconate titanate (PZT) was studied as to determine the piezoelectric activity to define the operating envelope with respect to temperature. The elastic properties $\left(c_{ijkl}^{E}\right)$, piezoelectric coefficients $\left(e_{ik}^{S}\right)$, dielectric properties $\left(\varepsilon_{ik}^{S}\right)$, and electro-mechanical coupling factors were determined as a function of temperature. The coupling factor k_{33} was found to be relatively constant to 200 °C and exhibit slight temperature dependence above 200 °C. The temperature sensitivity for both piezoelectric coefficient and electromechanical coupling factor were very small; the slopes $\Delta d_{31}^{T}/d_{31}^{T}$ and $\Delta k_{33}/k_{33}$ were found to be 0.01 and (−0.07) respectively in the range of 120 to 200 °C. This measurement technique will populate databases that describe the piezoelectric properties of commercially available PZT piezoelectric materials. It can also facilitate the assessment of new piezoelectric materials that are currently being developed for higher temperature applications.

Keywords High temperature PZT piezoceramic · Changes in electrical and mechanical properties with respect to temperature

1 Introduction

High-temperature piezoelectric materials have potential aeronautical applications in fuel and gas modulation to reduce emission and noise, active structural control of hot sections and multifunctional active components for future aeronautic structures. Piezoelectric materials that show operation at high temperature are essential for industrial competitiveness. Although the significance of piezoelectric materials for high temperature applications is recognized, a limited number of studies have been reported for the materials with high piezoelectric coefficients at high temperatures [4, 17–20, 22–24]. Notably Berlincourt et al. [22] considered PZT-4 polycrystalline regarding temperature dependency. Damjanovic [24] discusses at length polycrystalline piezoelectric materials concerning their temperature dependency. Turner et al. [23] considered resistivity changes with respect to temperature in a wide range of piezoelectric materials.

This work is supported by US Air Force grant F49620-03-1-0128.

Z. Gubinyi · C. Batur (✉)
Department of Mechanical Engineering,
University of Akron,
Akron, OH 44325-3903, USA
e-mail: batur@uakron.edu

A. Sayir · F. Dynys
NASA Glenn Research Center,
Cleveland, OH, USA

The temperature dependence of the dielectric permittivity and piezoelectric constants of single crystal $PbTiO_3$ have been calculated by Haun et al. [25] using the Landau–Ginzburg theory which is based on thermodynamic considerations. A good agreement was found at very low temperatures where the defect contributions were not present. Haun et al. [26] used the modified Davonshire form of the elastic Gibbs free energy to develop phenomenological thermodynamic theory and to predict temperature dependence of the dielectric permittivity and piezoelectric constants of the lead zirconate–titanate solid solution system [26]. The commercial piezoelectric ceramics are mostly engineered at and around the morphotropic phase boundary and the domain wall contribution to the piezoelectric response is the dominant extrinsic origin of the instability of the observed piezoelectric effect. The impurities, defects and their spatial distributions determine the formation of different oxygen cage tilting combinations (rotation, in-phase tilting, anti-phase tilting) and possibly ordering of cations [27]. Until these nano-structural attributes and their interaction with mesoscale microstructure understood and quantified, there is a need to investigate the piezoelectric and dielectric properties of piezoelectric ceramics at elevated temperatures to assess their upper use temperature. However, most studies have been limited to determination of dielectric properties at high temperatures to determine Curie temperature and very little data exist on the temperature dependence of the piezoelectric properties.

The present investigation reports data and observations on temperature dependent piezoelectric and dielectric properties of commercially available piezoelectric ceramics. Piezoelectric properties of several commercially available lead zirconate titanate (PZT) piezoelectric discs were measured as a function of temperature. The experiments were done to assess solely the temperature effect on piezoelectric properties; it does not address fatigue studies in ferroelectrics to describe load dependent aging. To assess the high temperature performance of piezoelectric materials, resonant analysis test procedure as described in IEEE standard [2] was utilized. The trend between anti-resonant and resonant frequencies of a vibration mode with temperature helps to predict the behavior of the coupling factors and permittivity. The proposed technique uses the resonant and the antiresonant frequencies but not the actual impedance or conductance values of the material tested. The paper reports the mechanical piezoelectric and dielectric properties calculated from the measured values of the resonant and anti-resonant frequency pairs of the first and second radial modes and the first thickness mode as a function of temperature. The results show that the results are under question above about 330 °C due to the limitations of the data evaluation approach.

2 Experimental set-up

Figure 1 shows the experimental set-up. Agilent 4294A LCR meter was used to measure the electrical impedance of the piezoelectric material in the 10 kHz–10 MHz frequency range. All communication and control programs between the computer and its peripherals were written in Labview 7.1 language. A Eurotherm 2404 temperature controller maintained the furnace set point temperature. The heating rates and set points were controlled via computer. Small variations in impedance can be measured with 1% accuracy if the environment temperature is within ±5 °C at which the calibration is done. Beyond this temperature range the manufacturer expects 2% accuracy.

An important aspect of impedance measurement system is the calibration of the test fixture. The Agilent 16089A text fixture was used because of its adaptability to a high temperature furnace. Test fixture frequency range was 5 Hz–100 kHz, a broader frequency range was required for this study. In order to assess the suitability of 16089A test fixture at higher frequencies, its response was compared to 16453A dielectric test fixture rated for the 40 Hz to 10 MHz frequency range. The difference in the measurement results were found negligible at room temperature. To compensate for this minor difference and to eliminate errors produced between the test fixture and the Agilent 4294A, fixture compensation calibration was performed using a standard calibration kit supplied by Agilent [7].

The temperature of the furnace was monitored and controlled by the Eurotherm 2404 Temperature Controller. The controller contains a pre-set Proportional-Integral-Derivative (PID) control and receives the temperature set-points from the PC via USB to RS-232 interface. The furnace, shown in Fig. 2, is rated for 1600 °C, manufactured by PCW&Design Co. The frequency measurements were repeated at the pre-defined temperatures from room temperature up to 400 °C. The temperature was increased at 4 °C per minute and samples were kept at each measuring temperature for at least 20 min before the impedance was measured in order to ensure thermal equilibrium.

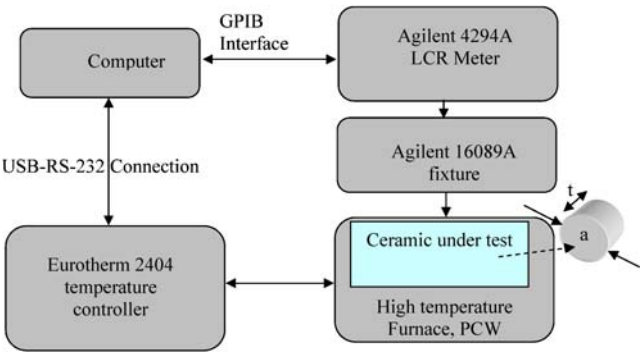

Fig. 1 Impedance measurements of ceramic for a frequency range of 40 Hz–110 MHz

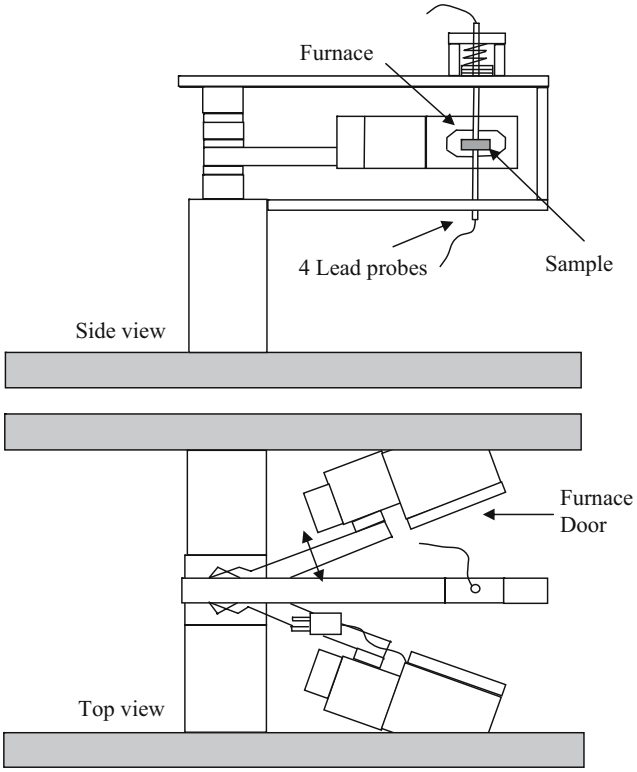

Fig. 2 High temperature piezoelectric measurement set-up

PZT samples were purchased from Piezo Kinetics Incorporated [8] and APC International [9]: (1) APC International – types APC850 PZT and APC880 PZT and (2) Piezo Kinetics Incorporated – Navy Type II – PKI-502. For all samples diameter to thickness ratio ranged between 10 and 12. Samples exposed to high temperatures may depolarize. Therefore, samples were measured only once through a thermal cycle to eliminate depolarization affects. To increase confidence in measurement of material coefficients with respect to temperature, it was decided to collect additional data with several different samples of the same material. This paper reports data in detail for Navy Type II samples but also highlights the characteristic trends for the APC880 PZT samples. APC850 PZT behaved similar to APC880 PZT.

3 Results and analysis

One way to quantify the effect of temperature on the piezoelectric material is to determine the elastic properties $\left(c_{ijkl}^{E}\right)$, piezoelectric coefficients (e_{kij}), dielectric properties $\left(\varepsilon_{ik}^{S}\right)$ and electro-mechanical coupling factor as a function of temperature. It is important to know changes of the coefficients of the constitutive equations [1–5] because they define the operating envelope with respect to temperature. Our procedure starts with the measurement of resonant and anti-resonant frequencies corresponding to radial and thickness modes of vibration. These frequencies were detected by a network analyzer within the frequency range of 10 kHz to 10 MHz. The poled PZT samples were subjected to controlled temperatures ranging from 25 to 400 °C. The resonant and anti-resonant frequency values were used to

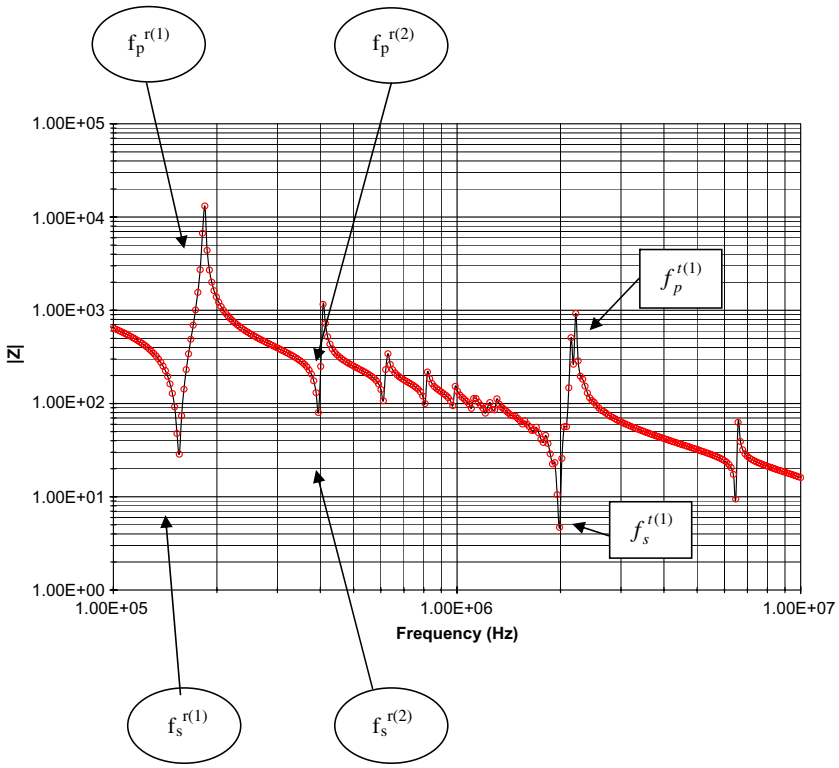

Fig. 3 Absolute impedance |*Z*| versus frequency for Navy Type II – PKI-502

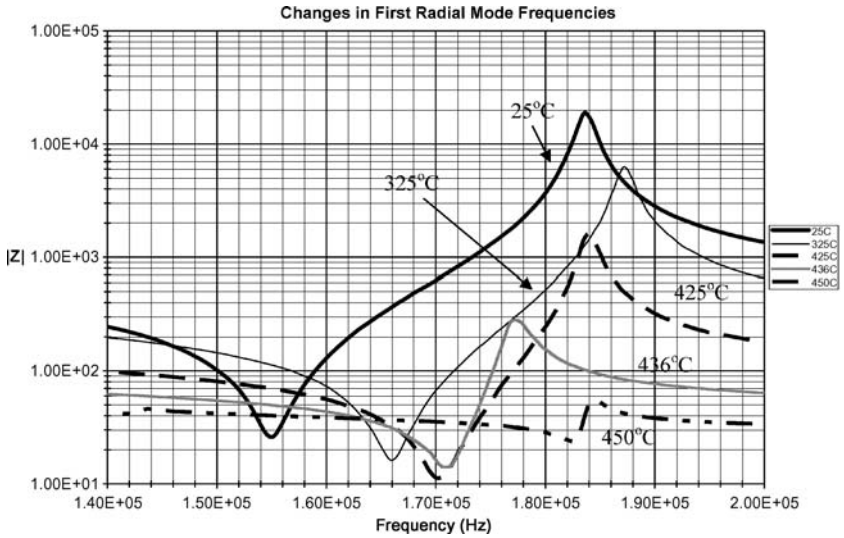

Fig. 4 First radial mode frequency shift with respect to temperature for Navy Type II PKI-502

determine the effect of temperature on the calculated piezoelectric parameters using accepted standard procedures [2, 4, 6]. Our work complements the study performed by Sheritt et al. [4] on BST-PT, BMT-PT and bismuth titanate (BT) samples. They determined that the bismuth titanate samples were stable up to 500 °C whereas BST-PT and BMT-PT samples were de-polarized below 500 °C.

3.1 Step I: Determination of resonant and antiresonant frequencies

The properties of the Navy Type II are listed in Appendix A for as received specimens. The measured resonant (f_s) and anti-resonant frequency (f_p) pairs correspond to different vibration modes $\left[\left(f_p^{r(1)},f_s^{r(1)}\right),\left(f_p^{r(2)},f_s^{r(2)}\right),\left(f_p^{t(1)},f_s^{t(1)}\right)\right]$ [10–13]. In notation, the superscript *r(i); i=1,2* refers to the first and second resonant frequencies of the *radial mode* and *t(1)* refers to the first *thickness mode* resonant frequency. The subscript *s* is used for the resonant frequency whereas *p* indicates the antiresonant frequency. In general, the symmetric vibration modes in circular piezoelectric ceramic disks have been classified as the Radial (*R*), Thickness (*T*), Edge (*E*), Anharmonic (*A*), Lamb (*L*), Thickness Shear (TS) and Thickness Extensional (TE) modes. Only the first two radial modes ($r^{(1)}$, $r^{(2)}$) and the first thickness mode ($t^{(1)}$) resonant behavior are significant for the samples used in this study; all of the electrical properties of the material was calculated based upon these modes [2].

Figure 3 shows the location of resonant and antiresonant frequencies at room temperature. Typical shifts in resonant frequencies from room temperature to 450 °C are shown in Fig. 4. The change in magnitude of the first radial mode impedance with increasing temperatures is representative of this type of material. The difference between the antiresonant and resonant frequencies decreased with increasing temperature. The changes in the antiresonant frequency $\left(f_p^{r(1)}\right)$ are not significant until the temperature approaches $T_C \approx 340\ °C$ at which $f_p^{r(1)}$ decreased significantly, then around $[T_C - 10\ °C]$ it starts to increase again along with $f_s^{r(1)}$ which shows more gradual increase until $[T_C - 20\ °C]$. This behavior can be observed in Figs. 4 and 5. The second radial mode and the first extensional mode show similar behavior as shown in Fig. 5.

3.2 Step II: determination of coefficients of the constitutive equations

All pertinent equations used in this section were taken from IEEE Standard on Piezoelectricity [2] or [6, 21]. Figure 5 shows the effect of temperature on the difference in resonance frequencies:

$$\Delta f = f_p^i - f_s^i;\ i = r1, r2, t1$$

The difference Δf diminishes as the temperature approaches to the Curie temperature for both in radial and thickness modes. This phenomenon also means that based upon the first mode frequencies $f_s^{r(1)}$ and $f_p^{r(1)}$, as the temperature gets closer to the Curie temperature, the planar coupling factor,

$$k_p^2 = \frac{\xi_1 J_0(\xi_1)/J_1(\xi_1) + \sigma^p - 1}{\xi_1 J_0(\xi_1)/J_1(\xi_1) - 2} \approx \frac{\left(f_p - f_s\right)\left[(\sigma^p)^2 - 1 + \eta_1^2\right]}{\left(2f_s - f_p\right)(1+\sigma^p) + \left(f_p - f_s\right)\left[(\sigma^p)^2 - 1 + \eta_1^2\right]} \quad (1)$$

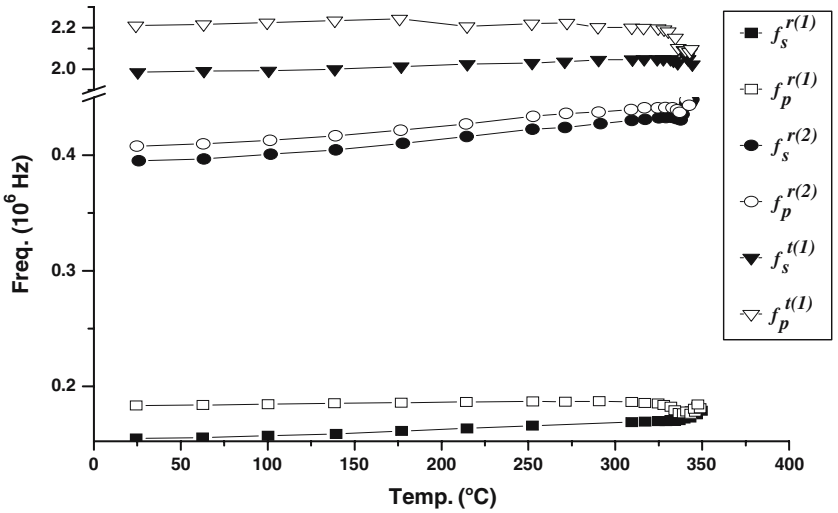

Fig. 5 PZT Sample, Navy Type II, PKI-502 resonant frequencies as a function of temperature

and the effective coupling factor,

$$k_{\text{eff}} = \sqrt{\frac{f_p^2 - f_s^2}{f_p^2}} \tag{2}$$

were expected to decrease. The planar coupling factor k_p was determined by using equations 120, 155 and Table 12 of IEEE Standard [2] where $\xi_1 = \eta_1 f_p / f_s$. The effective coupling factor k_{eff} describes the efficiency of conversion of electrical energy to mechanical and vice versa. In Eq. 1, the planar Poisson ratio $\sigma^p = s_{12}^E / s_{11}^E$ was defined as the ratio of elastic coefficients at constant electrical field E. A tenth order polynomial approximation was used to express σ^p as a function of $f_s^{r(2)} / f_s^{r(1)}$. Since the Poisson number depends only on the ratio of resonant frequencies, there was sensitivity in the calculations of these numbers. The impedance curves are typically squeezed horizontally at high temperatures (Fig. 4), therefore the location of resonant frequencies may not be well defined. The tabulated pair of numerical values for the σ^p and $f_s^{r(2)} / f_s^{r(1)}$ values from IEEE standard (Table 12 of reference [2]) were used to determine the coefficients of the polynomial which are given in Appendix B. The frequency constant η_1 in Eq. 1 is the lowest root of equation:

$$\eta_1 J_0(\eta_1) / J_1(\eta_1) = 1 - \sigma^p,$$

with $J_0(\eta_1)$, $J_1(\eta_1)$ representing the Bessel functions of zero and first order. A similar polynomial fit approach was also used to determine η_1 as a function of $f_s^{r(2)} / f_s^{r(1)}$. The polynomial fit uses the tabulated values given in IEEE standard [Table 12 of reference [2] and fits a sixth order polynomial as shown in Appendix C. Figure 6 shows the planar Poisson ratio σ^p that revealed some minor fluctuations

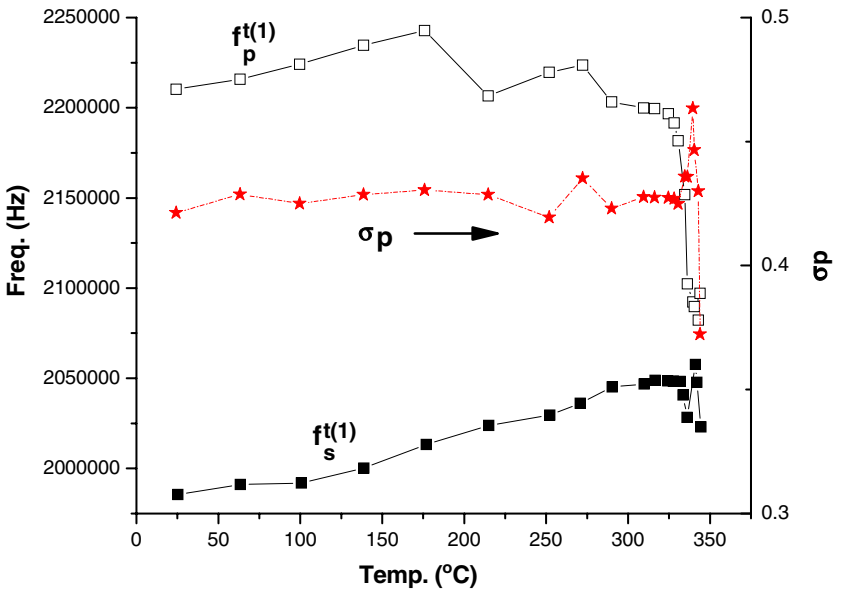

Fig. 6 PZT Sample, Navy Type II, PKI-502 σ_p, $f_s^{t(1)}$ and $f_p^{t(1)}$ vs. temperature

as the temperature increases, but in general it remains constant and below 0.5 throughout the temperature range.

The extensional mode coupling factor k_{31} was calculated from equation 116 in IEEE standard [2]

$$k_{31}^2 = \frac{k_p^2}{2(1-\sigma^p)} \tag{3}$$

The thickness–extensional mode coupling factor k_{33}^t was determined from equation 163 in IEEE standard [2] as

$$k_{33}^t = \sqrt{\frac{\pi}{2}\frac{f_s}{f_p}\tan\frac{\pi}{2}\frac{f_p^{t1}-f_s^{t1}}{f_p^{t1}}} \tag{4}$$

Figure 7 shows the values of k_{33}^t, k_{31}, k_p and k_{eff} coupling factors, which gradually decreased approaching to T_C and exhibited a steep decrease at the close vicinity of T_C.

The planar thickness–extensional mode permittivity component i.e., the dielectric constant ε_{33}^p is related to the dielectric constants ε_{33}^T and ε_{33}^S [Eqs. 106 and 157 of reference [2], i.e.,

$$\varepsilon_{33}^p = \varepsilon_{33}^T\left(1-k_p^2\right) \tag{5a}$$

$$\varepsilon_{33}^p = \varepsilon_{33}^S \Big/ \left[\left(1-k_{33}^t\right)^2\right] \tag{5b}$$

$$\varepsilon_{33}^p = \frac{-2_{31}^2}{s_{11}^E + s_{12}^E} + \varepsilon_{33}^T \tag{5c}$$

The dielectric permittivities ε_{33}^p, ε_{33}^T, ε_{33}^S should remain constant well below T_C and continually increase as T approaches T_C as predicted by the Curie–Weiss law. Figure 8 shows that for *PK502*, these coefficients remain relatively constant but show a very steep increase close to T_C at 340 °C. The maximum magnitude of ε for APC850 and APC880 rises to *8.8E−8*, *4.0E−8*, *2.8E−8 F/m* respectively around the Curie temperature with *PK502* exhibiting a very sharp rise in the permittivity. The PK502 also had the steepest slope of $\partial\varepsilon/\partial T = 0.00210\text{^} - 8$ in the temperature range of 25 to 100 °C. For the same temperature range the APC850 and APC880 (not shown) have $\partial\varepsilon/\partial T = 0.002 \times 10\text{^} - 9$ $\partial\varepsilon/\partial T = 0.011 \times 10 - 9$, respectively.

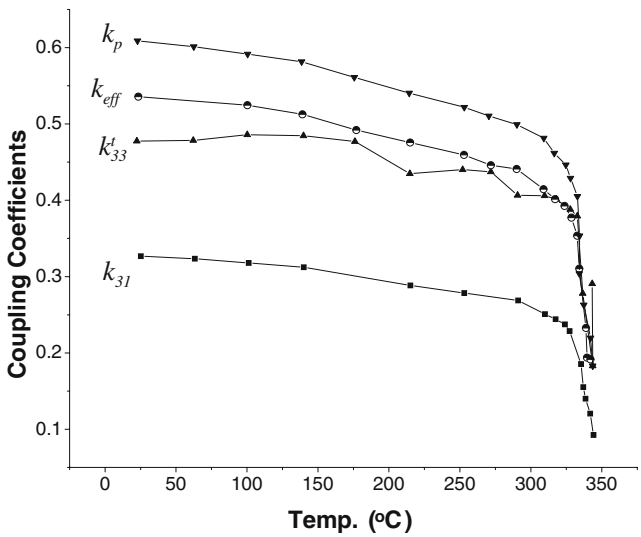

Fig. 7 PZT Sample, Navy Type II, PKI-502 k_{33}^t, k_{31}, k_p and k_{eff} vs. temperature

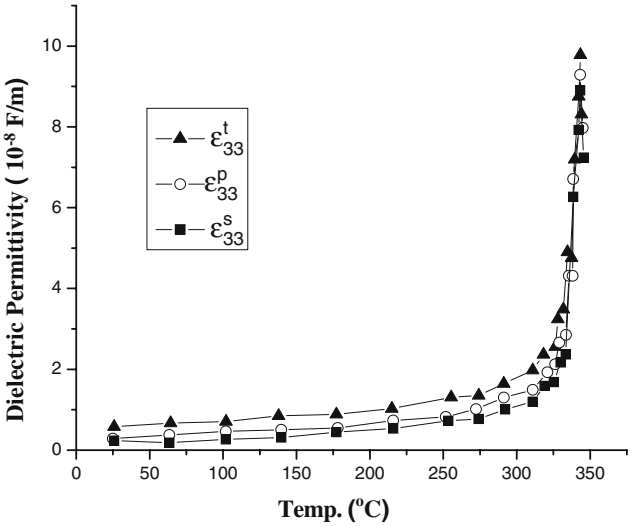

Fig. 8 PZT Sample, Navy Type II, PKI-502 ε_{33}^p, ε_{33}^T and ε_{33}^S vs. temperature

The piezoelectric effect for PK502 and APC850 ceramics engineered at the morphotropic phase boundary is a resultant of two physical phenomena, intrinsic and extrinsic contributions [14]. The intrinsic contribution originates from homogeneous deformation of the unit cell due to deformation caused by the elastic fields. Extrinsic contribution represents the elastic deformation caused by motion of domain walls and interphase interfaces. An extensive displacement (inverse piezoelectric effect) can be achieved through engineering the ceramic microstructure at the tetragonal/rhombohedral morphotropic phase boundary. The morphotropic phase boundary concept provides an increased number of polarization directions collectively enhancing the piezoelectric activity. Both of these intrinsic and extrinsic piezoelectric activities are temperature and frequency dependent. The decrease in piezoelectric properties for PK502 and APC850 with increasing temperature have been identified with a decline of the extrinsic contribution. As a comparison, the dielectric behavior as a function of temperature for purely tetragonal piezoelectric ceramics [15] possesses lower temperature dependent dielectric behavior compared to PK502 and APC850.

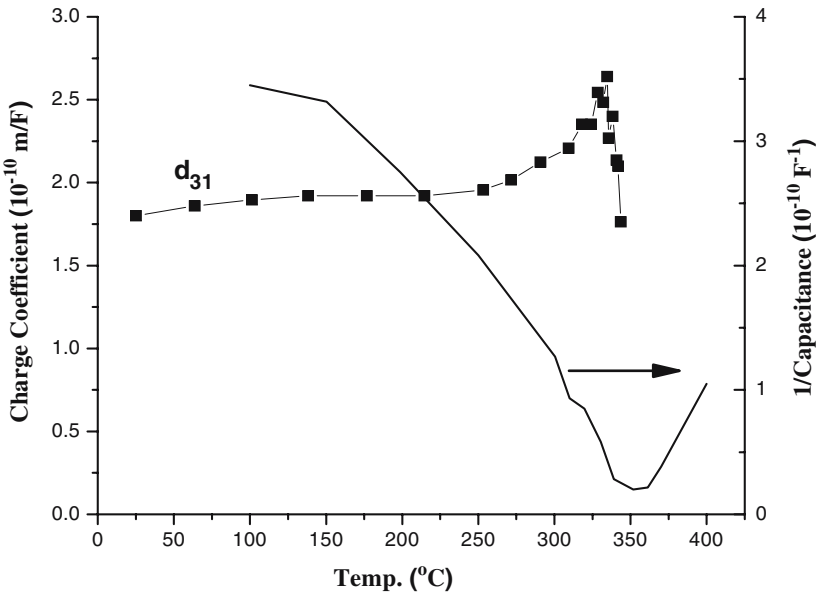

Fig. 9 PZT Sample, Navy Type II, PKI-502 d_{31} and (1/Capacitance) at 1 kHz vs. temperature (although 1/C is calculated for temperatures up to and exceeding 350 °C, values for over 350 °C are not physically meaningful)

Near the Curie temperature the dielectric, elastic, optical, and thermal constants of the piezoelectric ceramics show an anomalous behavior. This is due to a distortion in the crystal as the phase changes. The temperature dependence of the dielectric constant above the Curie temperature ($T > T_C$) in ferroelectric crystals is governed by the Curie–Weiss law:

$$\varepsilon = \varepsilon_0 \left(1 + \frac{C_1}{T - T_C}\right) \tag{6}$$

where ε_0 is the electric permittivity of free space and C_1 is the material specific Curie constant, T is the absolute temperature, and T_C is the Curie temperature. Low excitation voltage capacitance measurements are used at 1 kHz for the determination of material properties like the permittivity of a material. Based upon the measured capacitance at 1 kHz, the permittivity of the piezoelectric material is calculated by

$$\varepsilon = tC/A; \quad A = \pi a^2/4 \tag{7}$$

Where t is the distance between the electrodes, C is the capacitance and A is the area of an electrode. Based on Eqs. 6 and 7, the behavior of (1/C) is expected to reach its minimum around T_C as shown in Fig. 9.

Figure 9 also shows that the extensional mode piezoelectric constant d_{31} continuously increase with the temperature. However, the absolute value of the d_{31} remains stable until it reaches the vicinity of T_C then it drops significantly. This parameter is calculated from the following equation [2, 6]

$$\begin{aligned} &d_{31} = k_{31}\sqrt{\varepsilon_0 K_3^T s_{11}^E}; \\ &\varepsilon_0 = 8.85 \times 10^{-12} F/m; \quad K_3^T = C/(\varepsilon_0 A/t) \end{aligned} \tag{8}$$

The elastic coefficients s_{11}^E, s_{12}^E, and s_{11}^D are determined by:

$$\begin{aligned} &s_{11}^E = \frac{\eta_1^2}{\rho\left(2\pi f_s^{r(1)} a\right)^2 \left(1 - (\sigma^p)^2\right)}; \\ &s_{12}^E = -\sigma^p s_{11}^E \; ; \quad s_{11}^D = s_{11}^E - \frac{d_{31}^2}{\varepsilon_{cc}^T} \end{aligned} \tag{9}$$

Figure 10 compares the compliance characteristics of PZT 502 and APC 880. The lower compliance APC 880 with nominal s_{11}=1.1610^−11 m^2/N shows much more piezoelectric response than the higher compliance PZT 502 with the nominal s_{11}=1.810^−11 m^2/N.

The elastic coefficients c_{12}^p *and* c_{33}^E were calculated by Eqn. 161 of [2]

$$\begin{aligned} &c_{12}^p = -\frac{s_{12}^E}{\left(s_{11}^E\right)^2 - \left(s_{12}^E\right)^2}; \\ &c_{33}^E = 4\left(1 - \left(k_{33}^t\right)^2\right)\rho\left(f_p^{t1} t\right)^2 \end{aligned} \tag{10}$$

They remain relatively stable until the temperature reaches [T_C−*20 °C*], Fig. 11.

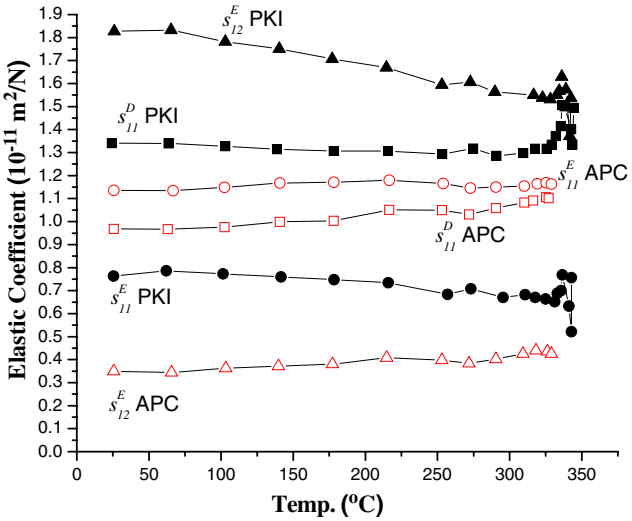

Fig. 10 PZT Sample, Navy Type II, PKI-502 elastic coefficients vs. temperature

Figure 11 also shows that the planar extensional mode piezo electric constant e^p_{31}, thickness extensional mode constant e_{33} values have the same trend as the d^t_{33} and d_{31}. They were calculated from Eq. 2

$$e^p_{31} = \frac{d_{31}}{s^E_{11} + s^E_{12}} \quad e_{33} = \sqrt{\varepsilon^S c^E k^2/(1-k^2)}; \tag{11}$$

Figure 7 shows the temperature dependence of the coupling factor k_{33} as a function of temperature up to 400 °C. The coupling factors were found to be nearly temperature independent up to 200 °C and exhibited slight temperature dependence above 200 °C. The k_{33} slightly decreased to 0.40. The temperature sensitivity for both piezoelectric coefficient and electromechanical coupling factor were very small; the slopes $\Delta d^T_{31}/d^T_{31}$ and $\Delta k_{33}/k_{33}$ were found to be 0.01 and (−0.07) respectively in the range of 120–200 °C. Finally, Fig. 12 shows the impedance parameter loss factor as a function of temperature. These values are determined by $Q = \text{Loss Factor} = \frac{|X|}{R} = \tan\Phi$ where Φ is the phase angle between the current and voltage as recorded by the network analyzer. It shows that the phase lag increases significantly with respect to temperature. The Q value of resonator which is defined as the bandwidth frequency of the resonant and antiresonant center in general increase with the temperature (not shown.)

In present work, we were not concerned with unipolar and/or bipolar electrical mechanical loading. It is also important to point out that the catastrophic failures can be related to the electrode–dielectric compatibility issues. More accurate use temperature can only then be estimated by investigation of the material properties during bipolar cycling under mixed electrical and electromechanical loading.

For the PZT systems with compositions close to morphotropic phase boundaries (the one we used in the experiments), oscillating interphase and/or a localized transition between the tetragonal and rhombohedral phases is expected to contribute substantially to piezoelectric activity. This extrinsic contribution is strongly affected by temperature. It is clear from the earlier studies that depolarization of PZT composition occurs at temperatures well below that maximum dielectric permittivity. For coupled properties, such as piezoelectricity elastic and

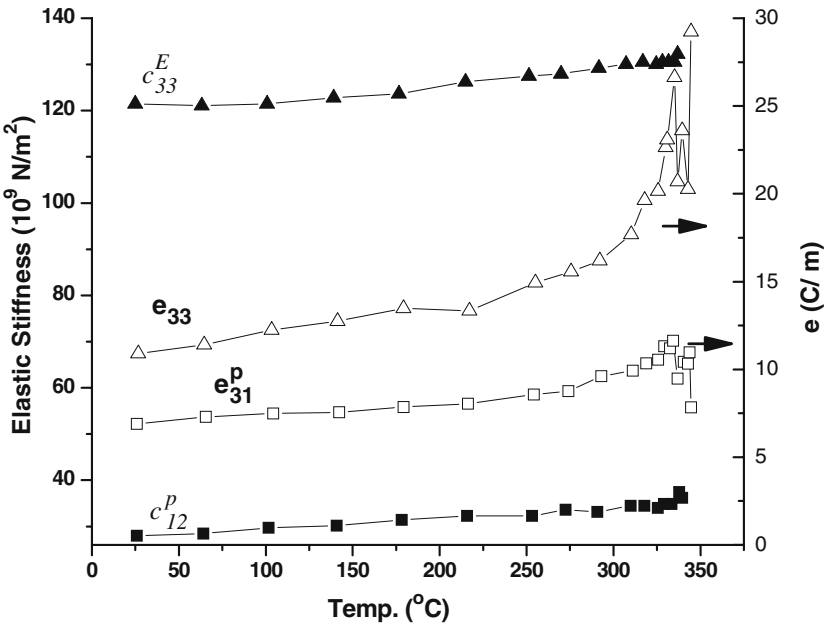

Fig. 11 PZT Sample, Navy Type II, PKI-502 c^p_{12}, and e^p_{31}, e_{33} and c^E_{33} vs. temperature

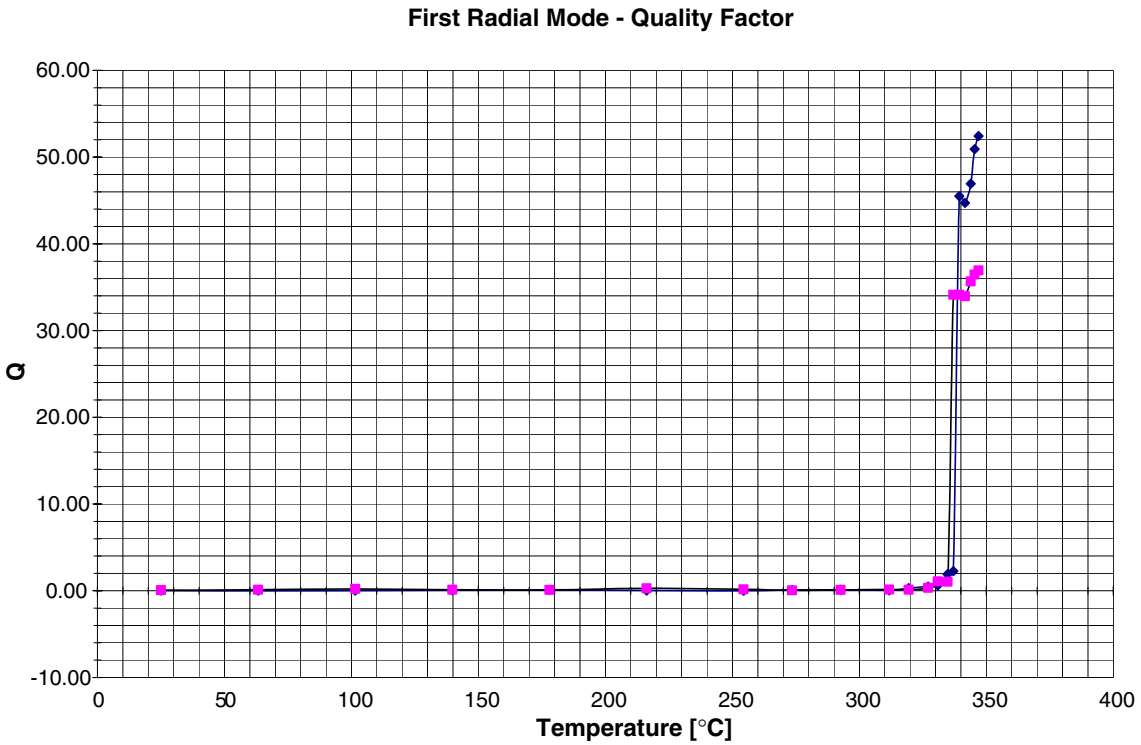

Fig. 12 The loss factor plot for Navy Type II, PKI-502

dielectric boundary conditions and the grain domains must be assessed. In the present investigation, piezoelectric ceramics were examined under weak alternating electric fields. Thus, the domain wall motion is expected to be reversible. The effect of domain wall dynamics on the dielectric, elastic and piezoelectric properties will be evaluated in future studies.

Domain wall are pinned in accordance with domain structure. According to Damjanovic and Newnham, [16] dipoles consisting of oxygen vacancies and associated dopant ions are able to be re-oriented in hard PZT. The decrease in coupling coefficients with increasing temperature can possibly be explained using volume theory, thus the degree of decrease is partly due to a gradual alignment of a doubly positively charged oxygen vacancy associated defect dipoles in the perovskite lattice. The critical experiments made by Warren et al. [28, 29] using electron paramagnetic resonance showed that the motion of oxygen vacancies are due to alignment oxygen vacancy related and thus agreed with the volume theory [30], which implies a reorientation of polar defect with respect to polarization direction. Warren et al. applied electrical field reaching up to 4.5 kV/cm in combination of time and temperature. In our investigation, we used very low electrical field in combination with temperature that exhibited measurable temperature dependence. Hence, we can not conclude the relative weight of temperature, electrical field and changing of electrical field direction, for the corresponding effect of the oxygen vacancy diffusion. Further considerations are needed to assess the orientation of the defect-dipoles with respect to spontaneous polarization direction. To understand the redistribution of charge may require the decoupling of electric field, temperature and strain field effects. To determine the exact mechanism, Hall measurements are necessary to assess the charge carrier concentration and mobility. It is also noteworthy that relaxation in ferroelectrics ceramics is not fully understood. It is clear from this limited experimental study that relaxation does not originate from an independent coupling between the dielectric mechanical losses in the material. In the evaluation of d_{31}, the effect of thermal expansion was neglected; the values of dimension and density of specimen were taken at room temperature.

4 Conclusion

The aeronautics and aerospace has been interested in high temperature piezoelectric materials as actuators and sensors for vibration control, shape control of aeronautical structures, noise reduction, adaptive flow control and active combustion control. The measurement system and the

metrology proposed in this work facilitate capturing changes in the resonant and anti-resonant frequencies and related electrical/mechanical properties as a function of temperature. The PZT samples studied show temperature dependent impedance and vibrational mode characteristics with significant changes occurring around T_C. There was a definite trend that the difference between anti-resonant and resonant frequencies of vibration modes do not increase with temperature which translate to reduced conversion efficiencies at high temperatures. The elastic properties $\left(c_{ijkl}^{E}\right)$, piezoelectric coefficients $\left(e_{ik}^{S}\right)$, dielectric properties $\left(\varepsilon_{ik}^{S}\right)$, and electro-mechanical coupling factors were determined as a function of temperature. The temperature dependent piezoelectric coefficient d_{33} was stable up to 200 °C. The coupling factor k_{33} was found to be relatively constant up to 150 °C and exhibited slight temperature dependence above 200 °C. The temperature sensitivity for both piezoelectric coefficient d_{31} and electromechanical coupling factor k_{33} were very small; the slopes $\Delta d_{31}^{T}/d_{31}^{T}$ and $\Delta k_{33}/k_{33}$ were found to be 0.01 and (−0.07) respectively in the range of 120 to 200 °C.

Acknowledgment Authors acknowledge and greatly appreciate the support from Case Western University/AFOSR subcontract F49620-03-1-0128.

Appendix A

Table 1 Properties of PZT Sample Navy Type II, PKI-502 at 25 °C

	Values listed by the Piezo Kinetics Inc.	Values measured in the laboratory
K^T Free relative dielectric constant	1,800	1,904
k_p Planar coupling factor	0.60	0.61
k_{31} Extensional mode coupling factor	0.34	0.33
$-d_{31}$ (m/V) Extensional mode piezoelectric constant C/N or m/V	175×10^{-12}	181×10^{-12}
Radius a (mm)	6.41	6.41
Thickness t (mm)	1.02	1.02

Appendix B. Approximation for σ^p

A tenth order polynomial approximation is used to express σ^p as a function of $f_s^{r(2)}/f_s^{r(1)}$.

$$\begin{aligned}\sigma^p = 100000000*\Big[&0.00002795314806*\left(f_s^{r(2)}/f_s^{r(1)}\right)^{10} - 0.00073437523227*\left(f_s^{r(2)}/f_p^{r(1)}\right)^{9}\\ &+0.00867731854159*\left(f_s^{r(2)}/f_s^{r(1)}\right)^{8} - 0.06072621017601*\left(f_s^{r(2)}/f_s^{r(1)}\right)^{7}\\ &+0.27874189616412*\left(f_s^{r(2)}/f_s^{r(1)}\right)^{6} - 0.87687338224803*\left(f_s^{r(2)}/f_s^{r(1)}\right)^{5}\\ &+1.91458077662298*\left(f_s^{r(2)}/f_s^{r(1)}\right)^{4} - 2.86495439332219*\left(f_s^{r(2)}/f_s^{r(1)}\right)^{3}\\ &+2.81186521683483*\left(f_s^{r(2)}/f_s^{r(1)}\right)^{2} - 1.63452106667819*\left(f_s^{r(2)}/f_s^{r(1)}\right)\\ &+0.4273285043911\Big]\end{aligned}$$

Appendix C. Approximation for η_1

A sixth order polynomial approximation is used to express η_1 as a function of $f_s^{r(2)}/f_s^{r(1)}$.

$$\begin{aligned}\eta_1 = 10000*\Big[&-0.00084523658921*\left(f_s^{r(2)}/f_s^{r(1)}\right)^{6}+0.01359048512994*\left(f_s^{r(2)}/f_s^{r(1)}\right)^{5}\\ &-0.09097672756895*\left(f_s^{r(2)}/f_s^{r(1)}\right)^{4}+0.32452162108606*\left(f_s^{r(2)}/f_s^{r(1)}\right)^{3}\\ &-0.65049087130736*\left(f_s^{r(2)}/f_s^{r(1)}\right)^{2}+0.69448273629625*\left(f_s^{r(2)}/f_s^{r(1)}\right)\\ &-0.30813284494365\Big]\end{aligned}$$

References

1. H.F. Tiersten, *Linear Piezoelectric Plate Vibrations* (Plenum, New York, 1969)
2. IEEE Standard on Piezoelectricity, ANSI/IEEE Std 176-1987. (The Institute of Electrical and Electronics Engineer, 1988)
3. J.W. Waanders, *Piezoelectric Ceramics Properties and Applications*, 1st edn. (Philips Components, Eidenhoven, Netherlands, 1991)
4. S. Sherrit, X. Bao, Y. Bar-Cohen, Z. Chang, Resonance Analysis of High Temperature Piezoelectric Materials for Actuation and Sensing, Paper 5387-58, Proceedings of the SPIE Smart Structures Conference San Diego, CA., Mar 14–18. 2004, SPIE Vol. 5387
5. A.H. Meitzler, H.M. O'Bryan Jr., H.F. Tiersten, Definition and Measurement of radial Mode Coupling Factors in Piezoelectric Ceramic Materials with Large Variations in Poisson's Ratio. IEEE Transactions on Sonics and Ultrasonics, SU-20, July 1973, pp 233–239
6. T.L. Jordan, Z. Ounaies, Piezoelectric Ceramics Characterization NASA/ CR-2001-211225 ICASE report to NASA Langley Research Center. Report No. 2001-28, September 2001
7. Agilent, *4294A Precision Impedance Analyzer Operation Manual*, 6th edn. (Agilent Technologies Japan, Ltd. Kobe Instrument Division, Part No. 04294-90050, November 2002)
8. Piezo Kinetics Incorporated, website: http://www.piezo-kinetics.com
9. APC International Ltd., website: http://www.americanpiezo.com
10. K. Okada, T. Sekino, *Agilent Technologies Impedance Measurement Handbook*, December 2003
11. J. Kocbach, Finite Element Modeling of Ultrasonic Piezoelectric Transducers; Influence of Geometry and Material Parameters on Vibration, Response Functions and Radiated Field, PhD Dissertation, the University of Bergen Department of Physics, September 2000
12. B. Jaffe, W.R. Cook Jr., H. Jaffe, *Piezoelectric Ceramics* (Academic Press, London, 1971)
13. A. Safari, R.K. Panda, V.F. Janas, *Ferroelectric Ceramics: Processing, Properties and Applications* (Department of Ceramic Science and Engineering, Rutgers University, Piscataway NJ, 1995) http://www.rci.rutgers.edu/~ecerg/projects/ferroelectric.html
14. Y. Xi, C. Zhili, L.E. Cross, J. Appl. Phys. **54**(6), 3399–3403 (1983)
15. S. Zhang, D.-Y. Jeong, Q. Zhang, T.R. Shrout, J. Cryst. Growth **247**, 131–136 (2003)
16. D. Damjanovic, R.E. Newnham, J. Intell. Mater. Syst. Struct. **3**, 190–208 (1992)
17. S. Sherrit, G. Yang, H.D. Wiederick, B.K. Mukherjee, Temperature Dependence of the Dielectric, Elastic and Piezoelectric Material Constants of Lead Zirconate Titanate Ceramics. Proc., of Int. Conf. on Smart Materials Structure and Systems, 7–10 July, 1999, Bangalore India, pp. 121–126
18. W. Ren, L. Han, R. Wicks, L. Yang, B.K. Mukherjee, Electric-field induced phase transitions of <001> oriented $Pb(Mg_{1/3}Nb_{2/3})O_3$-$PbTiO_3$ single crystals. Smart Structures Materials, Active Materials: Behavior Mechanics, SPIE Proc. **5761**, 272–278 (2005)
19. W. Ren, S.-F. Liu, B.K. Mukherjee, Appl. Phys. Lett. **80**(17), 3174–3176 (2002)
20. S. Zhang, D.-J. Jeong, Q. Zhang, T.R. Shrout, J. Cryst. Growth **247**, 131–136 (2003)
21. D.S. Campbell, A.M. MacSwan, Br. J. Appl. Phys. **12**, 188–192 (1961)
22. D.A. Berlincourt, D.R. Curran, H. Jaffe, Piezoelectric and piezomagnetic materials and their function in transducers *Physical Acoustics – Principles and methods*, Vol. I – Part A, ed. by W.P. Mason (Academic, New York, 1964)
23. R.C. Turner, P.A. Fuierer, R.E. Nenwham, T.R. Shrout, Appl. Acoust. **41**, 299–324 (1994)
24. D. Damjanovic, Curr. Opin. Solid State Mater. Sci. **3**, 469–473 (1998)
25. M.J. Haun, E. Furman, S.J. Jang, H.A. McKinstry, L.E. Cross, J. Appl. Phys. **62**(8), 3331–3338 (1987)
26. M.J. Haun, E. Furman, S.J. Jang, L.E. Cross, Ferroelectrics **99**, 63–86 (1989)
27. M.-H. Berger, A. Sayir, F. Dynys, P. Berger, Solid State Ion. **177** (26–32), 2339–2345 (2006)
28. W.L. Warren, D. Dimos, G.E. Pike, K. Vaheusden, Appl. Phys. Lett. **67**(12), 1689–1691 (1995)
29. W.L. Warren, K. Vaheusden, D. Dimos, G.E. Pike, B. Tuttle, J. Am. Ceram. Soc. **79**(2), 536–538 (1996)
30. P.V. Lambeck, G.H. Jonker, Ferroelectrics **22**, 729–734 (1978)